inorganics

Article

Efficient Catalytic Reduction of Organic Pollutants Using Nanostructured CuO/TiO_2 Catalysts: Synthesis, Characterization, and Reusability

Mariyem Abouri [1,2], Abdellah Benzaouak [3], Fatima Zaaboul [2], Aicha Sifou [2], Mohammed Dahhou [2], Mohammed Alaoui El Belghiti [1], Khalil Azzaoui [4,5], Belkheir Hammouti [5], Larbi Rhazi [6], Rachid Sabbahi [7,*], Mohammed M. Alanazi [8] and Adnane El Hamidi [2,*]

1 Laboratory of Spectroscopy, Molecular Modeling, Materials, Nanomaterial, Water and Environment, Faculty of Sciences, Mohammed V University in Rabat, Avenue Ibn Battouta, Rabat BP1014, Morocco; mariyemab@gmail.com (M.A.); m.elbelghiti@um5r.ac.ma (M.A.E.B.)
2 Laboratory of Materials, Nanotechnologies and Environment, Faculty of Sciences, Mohammed V University in Rabat, Avenue Ibn Battouta, Rabat BP1014, Morocco; zaaboul.fatima00@gmail.com (F.Z.); aichasifou@gmail.com (A.S.); m.dahhou@um5r.ac.ma (M.D.)
3 Laboratory of Spectroscopy, Molecular Modeling, Materials, Nanomaterials, Water and Environment, Environmental Materials Team, ENSAM, Mohammed V University, B.P. 765, Rabat 10090, Morocco; a.benzaouak@um5r.ac.ma
4 Engineering Laboratory of Organometallic, Molecular Materials and Environment, Faculty of Sciences, Sidi Mohammed Ben Abdellah University, UEMF, Fes 30000, Morocco; k.azzaoui@yahoo.com
5 Euromed Research Center, Euromed Polytechnic School, Euromed University of Fes, Eco-Campus, Fes Meknes Road, Fes 30030, Morocco; hammoutib@gmail.com
6 Institut Polytechnique UniLaSalle, Université d'Artois, ULR 7519, 19 rue Pierre Waguet, BP 30313, 60026 Beauvais, France; larbi.rhazi@unilasalle.fr
7 Research Team in Science and Technology, Higher School of Technology, Ibn Zohr University, Quartier 25 Mars, P.O. Box 3007, Laayoune 70000, Morocco
8 Department of Pharmaceutical Chemistry, College of Pharmacy, King Saud University, Riyadh 11451, Saudi Arabia; mmalanazi@ksu.edu.sa
* Correspondence: r.sabbahi@uiz.ac.ma (R.S.); adnane.elhamidi@fsr.um5.ac.ma (A.E.H.)

Abstract: The catalytic reduction of organic pollutants in water is a critical environmental challenge due to the persistent and hazardous nature of compounds like azo dyes and nitrophenols. In this study, we synthesized nanostructured CuO/TiO_2 catalysts via a combustion technique, followed by calcination at 700 °C to achieve a rutile-phase TiO_2 structure with varying copper loadings (5–40 wt.%). The catalysts were characterized using X-ray diffraction (XRD), attenuated total reflectance-Fourier transform infrared (ATR–FTIR) spectroscopy, thermogravimetric analysis-differential thermal analysis (TGA–DTA), UV-visible diffuse reflectance spectroscopy (DRS), and scanning electron microscopy with energy-dispersive X-ray spectroscopy (SEM–EDS). The XRD results confirmed the presence of the crystalline rutile phase in the CuO/TiO_2 catalysts, with additional peaks indicating successful copper oxide loading onto TiO_2. The FTIR spectra confirmed the presence of all the functional groups in the prepared samples. SEM images revealed irregularly shaped copper oxide and agglomerated TiO_2 particles. The DRS results revealed improved optical properties and a decreased bandgap with increased Cu content, and 4-Nitrophenol (4-NP) and methyl orange (MO), which were chosen for their carcinogenic, mutagenic, and nonbiodegradable properties, were used as model organic pollutants. Catalytic activities were tested by reducing 4-NP and MO with sodium borohydride ($NaBH_4$) in the presence of a CuO/TiO_2 catalyst. Following the in situ reduction of CuO/TiO_2, Cu (NPs)/TiO_2 was formed, achieving 98% reduction of 4-NP in 480 s and 98% reduction of MO in 420 s. The effects of the $NaBH_4$ concentration and catalyst mass were investigated. The catalysts exhibited high stability over 10 reuse cycles, maintaining over 96% efficiency for MO and 94% efficiency for 4-NP. These findings demonstrate the potential of nanostructured CuO/TiO_2 catalysts for environmental remediation through efficient catalytic reduction of organic pollutants.

check for updates

Citation: Abouri, M.; Benzaouak, A.; Zaaboul, F.; Sifou, A.; Dahhou, M.; El Belghiti, M.A.; Azzaoui, K.; Hammouti, B.; Rhazi, L.; Sabbahi, R.; et al. Efficient Catalytic Reduction of Organic Pollutants Using Nanostructured CuO/TiO_2 Catalysts: Synthesis, Characterization, and Reusability. *Inorganics* **2024**, *12*, 297. https://doi.org/10.3390/inorganics12110297

Academic Editors: Roberto Nisticò and Silvia Mostoni

Received: 17 October 2024
Revised: 15 November 2024
Accepted: 15 November 2024
Published: 19 November 2024

Copyright: © 2024 by the authors. Licensee MDPI, Basel, Switzerland. This article is an open access article distributed under the terms and conditions of the Creative Commons Attribution (CC BY) license (https://creativecommons.org/licenses/by/4.0/).

Keywords: titanium dioxide; catalysts; catalytic reduction; 4-nitrophenol; methyl orange; copper oxide

1. Introduction

Across the world, water and energy shortages represent urgent and increasingly severe global challenges. On a global level, over one billion people face the critical issue of not having access to clean drinking water, which is a necessity for human existence. Furthermore, more than two billion individuals lack proper sanitation facilities, resulting in almost two million annual fatalities due to diseases transmitted through impure water sources or insufficient sewage systems [1]. Water pollution occurs when the concentration of harmful chemicals or biological substances in a water body surpasses established standards, leading to adverse impacts on both human health and the natural environment [2].

Azo dyes and nitroaromatic compounds exhibit high stability and are known for their carcinogenic, mutagenic, and nonbiodegradable properties, posing a significant threat to human life, water quality, and the environment. These substances, such as Congo red, rhodamine B (RhB), and methyl orange (MO), are extensively used in numerous chemical sectors, including paper, textiles, paint, and plastics. These industrial processes produce significant quantities of dyes, leading to the emergence of dye-laden particles that are introduced directly into the environment [3,4]. MO, for example, is a highly toxic and nonbiodegradable azo. The adverse effects of this toxic dye may disrupt the balance of water within ecosystems and pose health risks, including symptoms such as vomiting, diarrhea, breathing difficulties, and nausea [5]. In particular, 4-Nitrophenol (4-NP) is a highly toxic compound that is challenging to degrade and treat effectively [6].

Compared with alternative methods, nitrophenol and dye reduction in the presence of a suitable catalyst and sodium borohydride ($NaBH_4$) is a recommended protocol, since it is relatively more affordable, secure, and environmentally friendly [7–9]. Therefore, the exploration of techniques such as chemical reduction to efficiently degrade diverse chemical pollutants is of considerable interest. However, this method commonly faces a challenge in achieving a fast degradation rate at lower concentrations of reducing agents, such as sodium borohydride. Consequently, to minimize the quantity of reducing agent required and increase the reaction rate, the development of an efficient catalyst for this chemical reduction becomes crucial [10,11]. Owing to their exceptional physicochemical proprieties, there has been significant interest in the field of catalysis regarding transition and noble metal nanoparticles in recent years [12–16]. Among these materials, copper nanoparticles (CuNPs) have gained recognition as excellent materials that exhibit novel physiochemical characteristics. This has prompted their investigation in various applications, including catalysis, sensors, photocatalysis, diverse biological activities, energy storage, and organic synthesis applications [17–21]. The catalytic activity is closely related to the degree of dispersion of the Cu(NPs), and a superior performance has been noted with smaller-sized nanoparticles [22,23].

One significant challenge in employing nanoparticles as catalysts involves their agglomeration and accumulation, resulting in a decrease in their catalytic efficiency. A viable solution to address this concern is the utilization of solid supports to stabilize the nanoparticles [24]. For this purpose, a series of solid supports, such as polymers, metal oxides, and carbon materials [25–28], have been adopted to avoid sintering, enhance stability, and facilitate the optimal mobilization/dispersion of nanoparticles, aiming to maximize catalytic activities across a wide variety of applications. Among these supports, the immobilization of CuNPs on TiO_2, which is a representative n-type semiconductor material, has been extensively used as a photocatalyst, catalyst support, and cocatalyst because of its high oxidation ability, environmental friendliness, physicochemical stability, and cost effectiveness [29,30]. Research on the use of Cu/TiO_2 for catalytic reduction has gained significant attention because of its promising applications in environmental remediation. One study focused on synthesizing $Cu\text{-}TiO_2$ nanoparticles from the extract of Phoenix

dactylifera. These catalysts effectively degraded dyes, such as RhB, in 11 min and MO in 25 min, achieving reductions of 89.8 and 95.3%, respectively, with 21.3 mg/mL of the catalyst [31]. Other investigations explored various shapes and sizes of Cu nanostructures and revealed that smaller particles and specific morphologies enhanced the catalytic activity for nitroaromatic reduction [32]. Additionally, Cu/TiO_2 catalyst synthesized from *Chimonanthus praecox* extract exhibited superior performance in degrading pollutants, such as 4-nitrophenol and other organic dyes, with 10 mg of catalyst [33]. CuO/TiO_2 composite created using *Tilia platyphyllos* extract also demonstrated high catalytic activity, reducing MO in 10 min and methyl blue in 9 min with 3 mg of the catalyst [34]. Recent studies of CuO/TiO_2 nanocomposite have further highlighted their exceptional catalytic performance, particularly under direct sunlight, where these photocatalysts effectively drive the selective hydrogenation of 4-NP to 4-AP in the presence of $NaBH_4$ [35]. Moreover, binary CuO/TiO_2 composites have demonstrated excellent reactivity in tandem hydrogenation processes for nitro compounds [36].

In the present study, different wt.% CuO/TiO_2 (rutile) were synthesized through the combustion technique followed by calcination at 700 °C to ensure a complete transition from anatase to rutile. The prepared catalysts were characterized via X-ray diffraction (XRD), UV–vis diffuse reflectance spectroscopy, attenuated total reflectance–Fourier transform infrared (ATR–FTIR) spectroscopy, thermogravimetric analysis-differential thermal analysis (TGA–DTA), and scanning electron microscopy with energy-dispersive X-ray spectroscopy (SEM–EDS). The catalytic performance of CuO/TiO_2 was evaluated afterwards via the reduction of MO and 4-nitophenol as models of organic contaminants in the presence of $NaBH_4$. The influence of parameters, including $NaBH_4$ concentration, catalyst mass and reusability of the catalyst, were examined.

2. Results and Discussion

2.1. X-Ray Diffraction

The XRD patterns of the CuO/TiO_2 catalyst series are presented in Figure 1. The results obtained reveal that the materials are primarily composed of the rutile phase of TiO_2 in accordance with ICDD 21-1276. The presence of CuO in its monoclinic form was also verified in accordance with the ICDD 48-1548 reference pattern, confirming the effective loading of copper oxide in TiO_2. Figure 1 also reveals a correlation between the deposited quantity of Cu(II) ions and the intensities of the characteristic CuO peaks. These findings collectively indicate the successful preparation of the CuO/TiO_2 catalysts with varying percentages of CuO deposition. The average crystallite size of CuO was determined to be 26, 27, 32, 35, 36 nm for 40, 30, 20, 10 and 5 wt.% CuO/TiO_2 catalysts, respectively. The crystallite size was determined using the Scherrer equation [37]:

$$L = \frac{0.9\lambda}{\beta \cos\theta}$$

where λ is the X-ray wavelength (0.1540 nm), β is the full width at half maximum (FWHM), θ is Bragg's angle, and L represents the average crystallite size.

On the other hand, the absence of the anatase phase of TiO_2 is due to its transformation to rutile upon heating at 700 °C, as observed in Figure 2, which shows the XRD curves for the 40 wt.% CuO/TiO_2 catalysts subjected to various calcination temperatures. The primary difference observed was the phase transition of TiO_2 from anatase (ICDD 21-1272) to rutile (ICDD 21-1276), with complete transformation occurring at 700 °C. The same results were observed in many previous studies [38].

Following the reduction experiment using $NaBH_4$, the rutile structure of TiO_2 remained unchanged, indicating its stability under the reaction conditions. However, the monoclinic structure of CuO significantly decreased, leading to the formation of Cu(NPs), as depicted in Figure 3. Notably, two additional peaks emerged at 43.28° and 50.37°, corresponding to the (111) and (200) planes, respectively. These peaks are characteris-

tic of the face-centered cubic (FCC) crystal structure of metallic copper nanoparticles (ICDD No. 04-0836). The average Cu(NP) size is about 15 nm.

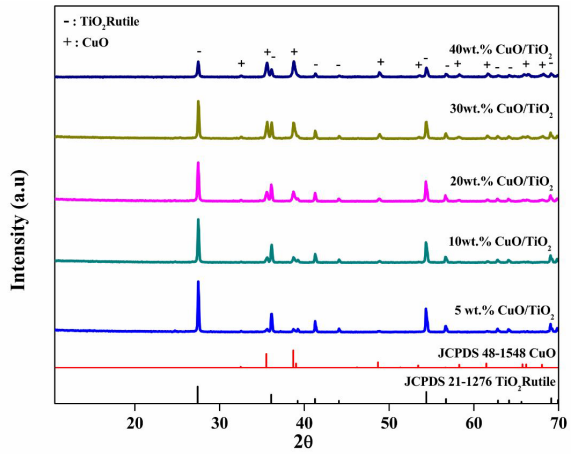

Figure 1. XRD patterns of different wt.% CuO/TiO_2 samples.

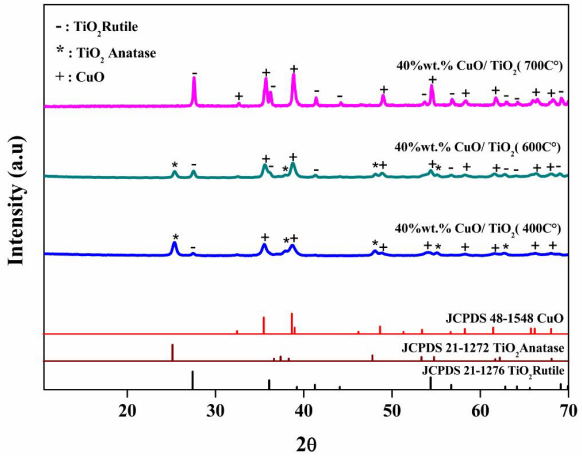

Figure 2. XRD patterns of 40 wt.% CuO/TiO_2 samples calcined at different temperatures.

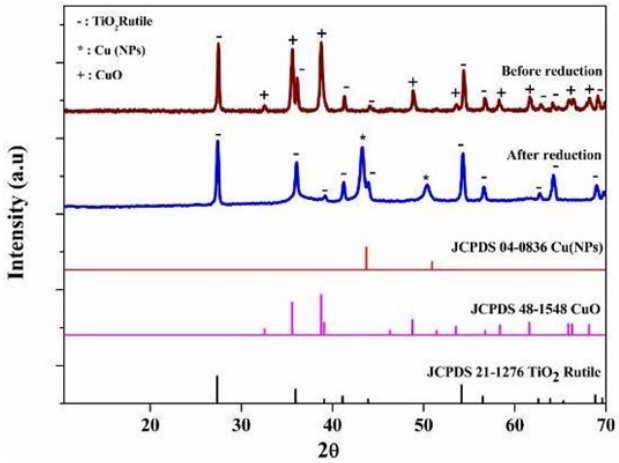

Figure 3. XRD patterns of 40 wt.% CuO/TiO_2 before and after the reduction experiment.

2.2. Thermal Analysis Measurement

To examine the thermal behavior of CuO/TiO_2, thermal experiments involving thermogravimetric and differential measurements were performed. The results are shown in Figure 4. The initial step, characterized by a weight loss of 3% within the temperature range

of 30 to 150 °C, can be attributed to the vaporization of water [39]. The notable weight reduction occurring between 200 and 350 °C, as evaluated at 30%, appears to be associated with the decomposition and combustion of the organic constituents. The latter was confirmed by an intense exothermic peak observed in the DTA curve and two intense peaks in the DTG curve [40]. On the other hand, no weight loss was observed at temperatures above 450 °C, and the anatase to rutile phase transition that should occur above 600 °C [38] was not observed in the DTA curve because of its reduced sensitivity compared with that of differential scanning calorimetry (DSC).

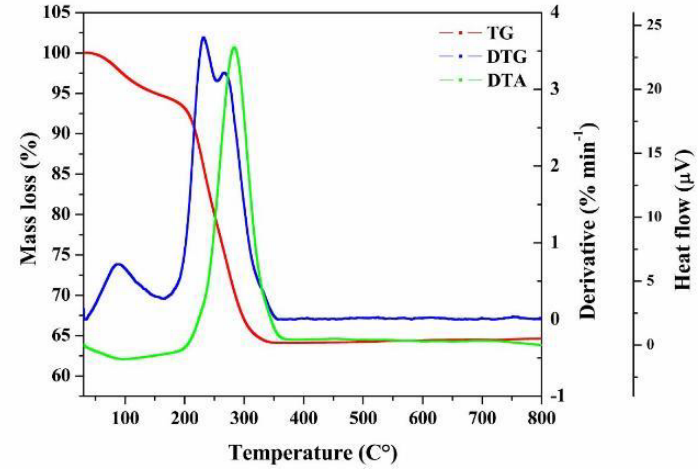

Figure 4. Thermal curves of the as-prepared 40 wt.% CuO/TiO_2 without calcination under air flow at 10 °C min^{-1}.

2.3. ATR–FTIR Spectroscopy

ATR–FTIR spectroscopy was performed on the catalysts calcined at 700 °C. The measurements were conducted across the spectrum ranging from 400 to 4000 cm^{-1}, and the results are shown in Figure 5. The analysis revealed similar results for the different catalysts with different percentages of CuO. The absence of water molecules and other contaminants in the catalyst was confirmed by the observation of strong bands in the infrared spectrum just below 1000 cm^{-1}. These bands typically correspond to lattice vibrations within metal oxides. The peak observed at approximately 650 cm^{-1} is associated with the presence of the Ti-O-O stretching vibration bond. Additionally, the spectra revealed two other distinct bonds below 500 cm^{-1} that were attributed to metal–oxygen (M–O) bond vibrations. All the observed bands suggest the existence of both Ti–O vibrational stretching and Cu–O stretching vibration bonds [41], which confirms the successful incorporation of CuO into TiO_2.

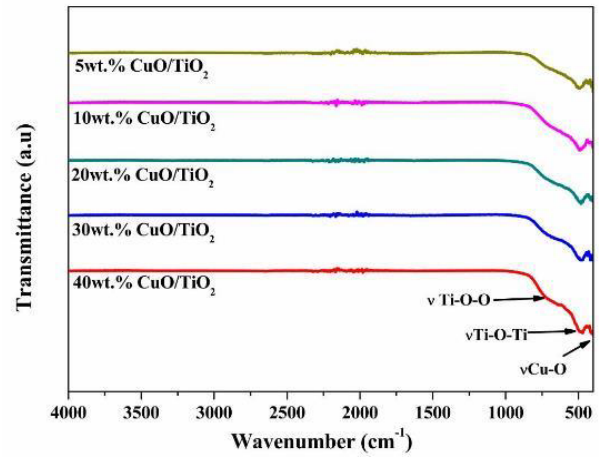

Figure 5. Infrared spectra of the wt.% CuO/TiO_2 samples.

2.4. UV–Vis Diffuse Reflectance Spectroscopy

Figure 6a presents the diffuse reflectance spectroscopy (DRS) results for TiO_2 and the various wt.% CuO/TiO_2 catalysts, revealing their optical properties in the 200–800 nm range. TiO_2 exhibits a pronounced absorption peak below 400 nm, which is attributed to its intrinsic interbond absorption [42]. In contrast, the spectrum of the wt.% CuO/TiO_2 catalysts displays additional absorption bands in the 400–800 nm range. The absorption band between 400 and 600 nm is attributed to charge transfer from the valence band (VB) of TiO_2 to CuO. Additionally, the lower absorption band within the 500–800 nm range is associated with the intrinsic exciton band of CuO and the d–d transition of Cu^{2+} species [43]. The band gap energies (Eg) of TiO_2, CuO, and the different wt.% CuO/TiO_2 catalysts were determined by identifying the intersection of the linear portion of the $(\alpha hv)^2$ vs. energy (eV) curves, as detailed in Figure 6b. The Eg values for TiO_2 and wt.% CuO/TiO_2 are summarized in Table 1. These results indicate that increasing the CuO content leads to a progressive narrowing of the band gap. This trend can be attributed to the incorporation of Cu, which introduces additional energy states within the band structure, thereby lowering the bandgap. The reduced bandgap in the CuO/TiO_2 catalysts enhances their visible light absorption, which is beneficial for photocatalytic applications [44].

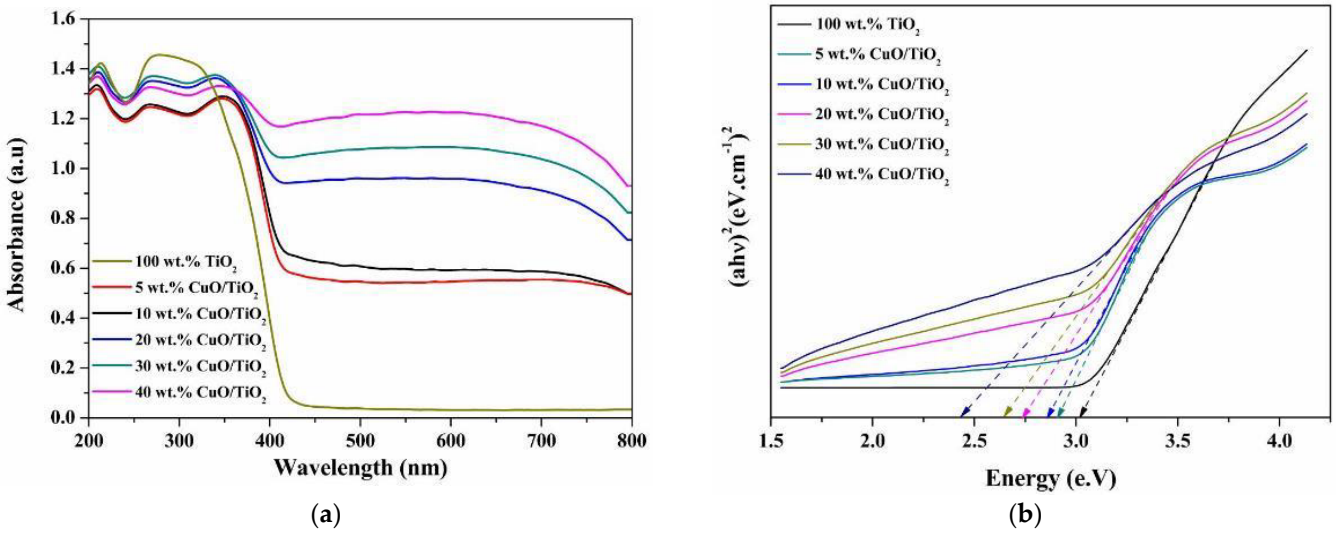

Figure 6. (**a**) UV–vis diffuse reflectance spectra of TiO_2 and wt.% CuO/TiO_2 and (**b**) Tauc plot.

Table 1. Bandgaps of different catalysts.

Catalyst	TiO_2	5 wt.% CuO	10 wt.% CuO	20 wt.% CuO	30 wt.% CuO	40 wt.% CuO
Band gap (eV)	3.02	2.91	2.86	2.73	2.65	2.43

2.5. SEM–EDS Analysis

Morphological studies via SEM–EDS were carried out on the CuO/TiO_2 catalyst. Figure 7 shows representative SEM images of synthesized CuO/TiO_2, which reveal a homogeneous spherical morphology with varying diameters and numerous micrometer-sized particles. Additionally, the catalyst has a porous structure and some aggregation of spheres. The analysis of the CuO/TiO_2 catalyst via energy dispersive X-ray (EDX) spectroscopy aimed to examine the presence and distribution of copper, titanium, and oxygen within the material. The EDX spectrum of CuO/TiO_2 is shown in Figure 8, and the results indicate the successful incorporation of copper into the TiO_2 sample. Additionally, the elemental mapping analysis revealed a uniform distribution of copper (depicted in yellow), titanium (represented in pink), and oxygen (shown in blue) in the samples, as illustrated in Figure 9.

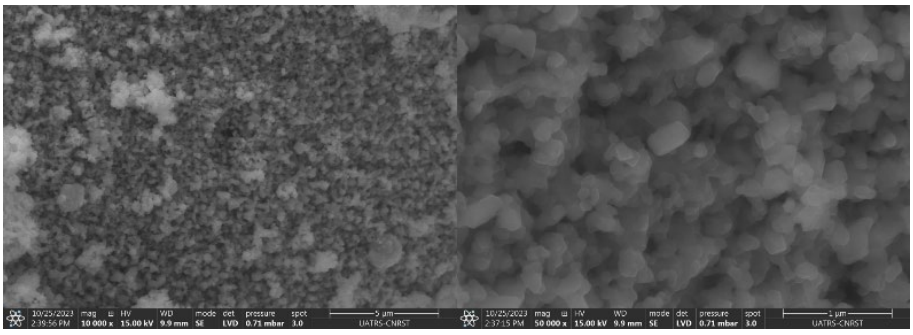

Figure 7. SEM micrographs of 40 wt.% CuO/TiO_2.

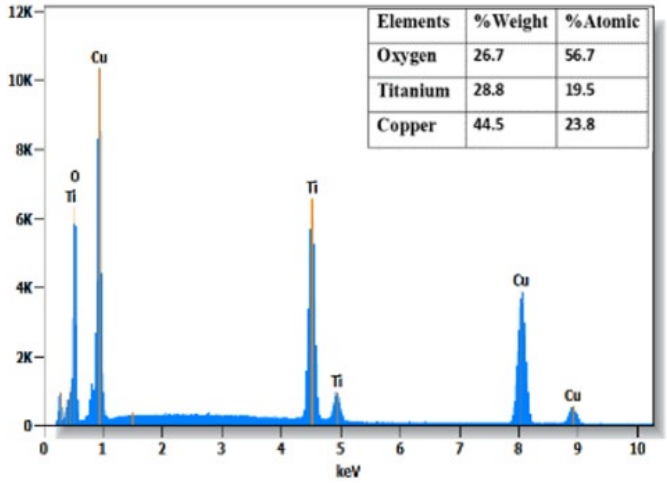

Figure 8. EDS Spectrum of 40 wt.% CuO/TiO_2.

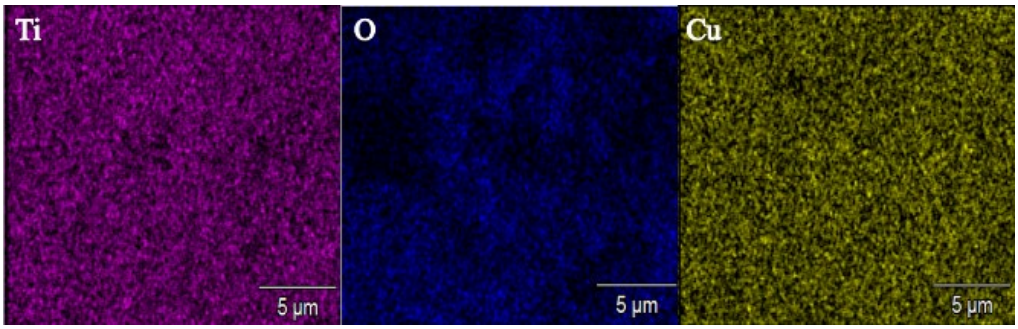

Figure 9. EDX mapping of the 40 wt.% CuO/TiO_2 catalyst.

2.6. Catalytic Reduction of 4-NP and MO by a CuO/TiO_2 Catalyst

The catalytic performance of the CuO/TiO_2 samples with different CuO loadings (5 to 40 wt.%) was evaluated for the reduction of organic pollutants via $NaBH_4$, as shown in Figure 10a,b. As shown in Figure 10a, which represents the reduction of 4-nitrophenol (4-NP), the 40 wt.% CuO/TiO_2 catalyst exhibited the fastest catalytic activity, reaching nearly 100% removal within a shorter reaction time than the other catalysts and pure CuO. Similarly, in Figure 10b, which shows the reduction of MO, 40 wt.% CuO/TiO_2 again demonstrates the fastest catalytic performance. The pure CuO sample exhibited lower catalytic activity than the 40 wt.% CuO/TiO_2 sample did, likely due to the agglomeration of copper oxide nanoparticles, which reduced the number of accessible active sites. On the other hand, at lower CuO loadings (e.g., 5 wt.%), the catalytic activity is the slowest, which can be attributed to the lower number of active CuO/TiO_2 sites available for the reduction process.

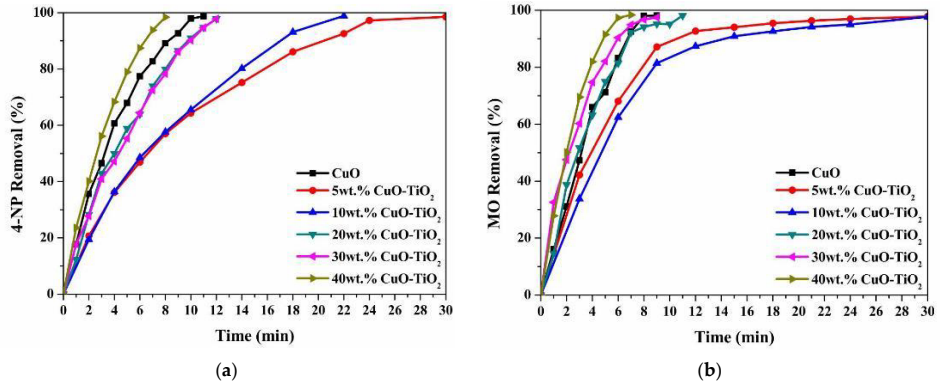

Figure 10. Reduction performance of the wt.% CuO/TiO_2 catalysts for 4-NP (**a**) and MO (**b**).

Figure 11a,b display the absorption spectra of 4-NP and MO in the presence of $NaBH_4$ but without the use of a catalyst. Under these conditions, the peak intensities show little change even after 180 min, indicating a negligible reduction rate, as no significant degradation occurred during this time. However, when CuO/TiO_2 is introduced alongside $NaBH_4$ (Figure 11c,d) and forming $Cu(NPs)/TiO_2$, a rapid and noticeable reduction in the characteristic absorption peaks of both 4-NP and MO is observed. For 4-NP, the peak at ~400 nm diminished progressively, vanishing completely within 480 s (Figure 11c). Similarly, the absorption peak of MO at approximately 464 nm disappears within 420 s (Figure 11d). This demonstrates a much faster and more efficient reduction process in the presence of the CuO/TiO_2 catalyst than in the presence of $NaBH_4$ alone. Simultaneously, a pair of new peaks emerged at 297 nm and 231 nm for the reduction of 4-NP and at 242 nm during the reduction of MO. These new peaks can be attributed to the characteristic absorption bands of the colorless 4-aminophenol (4-AP) from 4-NP and sulfanilic acid along with dimentyl-4-phenylenediamine from OM [45,46].

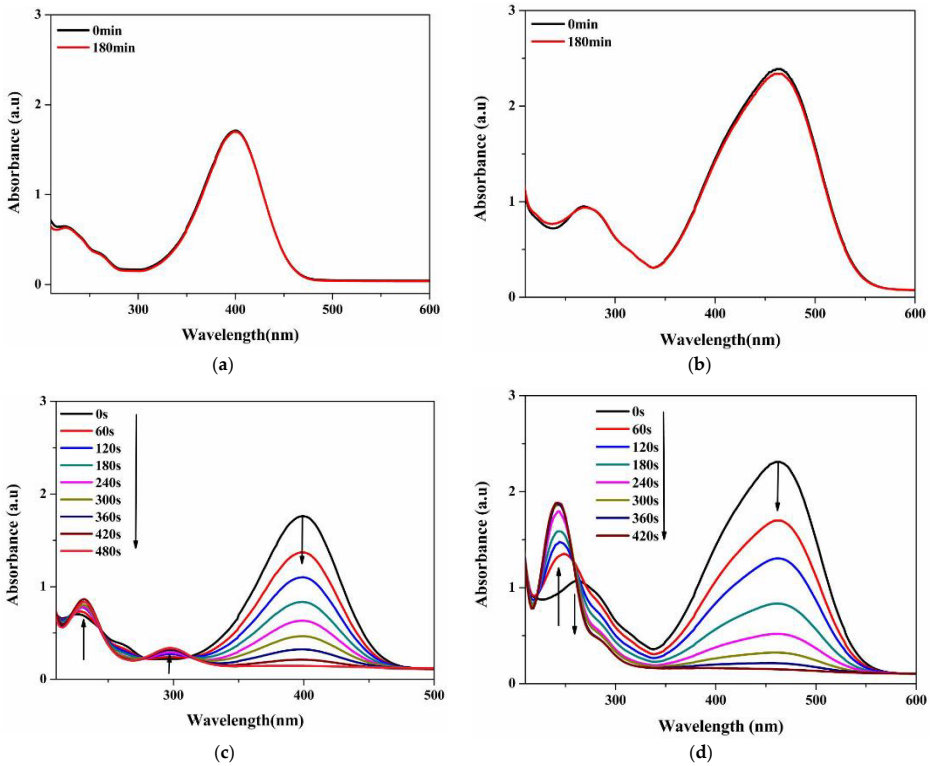

Figure 11. UV–vis spectra of the reduction of (**a**) 4-NP and (**b**) MO by $NaBH_4$ without the catalyst and absorbance spectra of (**c**) 4-NP and (**d**) MO in the presence of $NaBH_4$ and CuO/TiO_2.

2.6.1. Kinetic Study

The pseudo-first-order kinetic model of Langmuir–Hinshelwood was employed to analyze the kinetics data due to the substantial excess of $NaBH_4$ compared with the organic dyes, denoted as ([$NaBH_4$]/[Pollutant]) = 40. The rate constants (k_{app}) governing the conversion reactions for both 4-NP and MO were determined via the following equation:

$$\ln\frac{C_t}{C_0} = \mathrm{Ln}\frac{A_t}{A_0} = -k_{app}t \quad (1)$$

As depicted in Figure 12a,b, the Ln (A_t/A_0) vs. time of reaction was determined by analyzing the absorption peak intensities at 400 nm (4-NP) and 464 nm (MO). Remarkably, the reduction process was initiated promptly, devoid of any induction time requirement. The graphical representation of Ln (A_t/A_0) against time exhibited a robust linear correlation, aligning well with the expectations of pseudo-first-order kinetics. Consequently, the calculated rate constants were determined to be 0.00517 s^{-1} for 4-NP and 0.00727 s^{-1} for MO. To enable a comparative assessment of CuO/TiO_2 performance, an activity factor denoted as k' was computed via the following equation:

$$k' = \frac{k_{app}}{m} \quad (2)$$

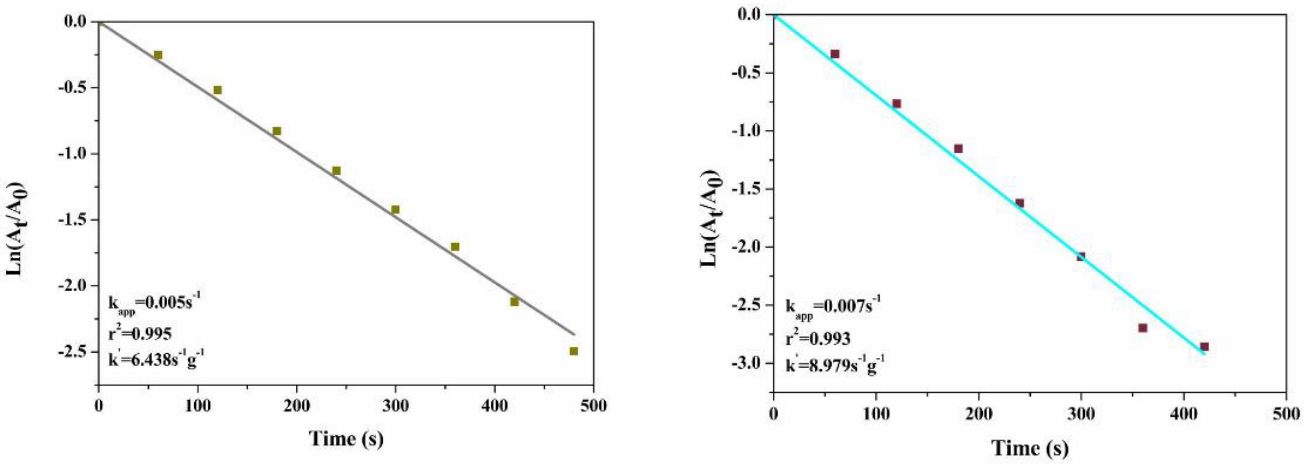

(**a**) (**b**)

Figure 12. First-order plot for the catalytic reduction of (**a**) 4-NP and (**b**) MO. Experimental conditions: 40 wt.% CuO/TiO_2 dose = 0.04 g/L, [$NaBH_4$] = 14 mM, and [4-NP or MO] = 0.35 mM.

In this equation, m(g) represents the mass of the copper in the catalyst involved in the reaction.

In this context, the derived k′ values were 6.46 s^{-1} g^{-1} for 4-NP and 8.98 s^{-1} g^{-1} for MO. For a comprehensive comparison, Table 2 illustrates the varying efficacies of Cu(NPs) catalysts documented in the literature.

Tables 3 and 4 show an increase in the observed rate constants (k_{app}) with increasing CuO percentage in the catalyst. The 40 wt.% CuO/TiO_2 catalyst exhibits the highest rate constant (0.005 s^{-1}), indicating that a higher copper loading favors faster reduction kinetics for 4-NP and MO. However, when considering the mass of active copper in the catalyst, the normalized values (k′) indicate that the 5 wt.% CuO/TiO_2 catalyst exhibits the highest activity (17.5 $s^{-1}g^{-1}$). This suggests that, although increasing the CuO loading accelerates the overall reaction, the efficiency per unit mass of copper is maximized at lower loadings.

After the in situ reductive reaction of CuO/TiO_2 to Cu (NPs)/TiO_2 with $NaBH_4$, an underlying mechanism enables the catalytic reduction of 4-NP and MO using Cu(NPs)/TiO_2 in the presence of $NaBH_4$ (Figure 13). In this process, the BH^{4-} ions adhere to the surface of the catalyst, thereby initiating the creation of BO^{2-} through the self-hydrolysis

of $NaBH_4$. Moreover, BH^{4-} interacts with the catalyst, facilitating the transfer of active hydrogen species, leading to the formation of an energetically charged hydrogen layer on the catalyst surface [47]. The organic pollutants subsequently attach themselves to the catalyst surface, undergoing reduction into 4-AP for 4-NP and sulfanilic acid along with dimentyl-4-phenylenediamine for MO during the step that governs the reaction rate. The produced compounds are then desorbed from the surface of the Cu(NPs)/TiO_2 catalyst. As a result, Cu(NPs)/TiO_2 exhibits highly efficient catalytic reduction due to the supply of electrons to the catalyst by BH_4^- ions, a mechanism that enables 4-NP and MO to bond with the catalyst surface, consequently yielding enhanced catalytic activity [48].

Table 2. Comparison of the catalytic properties of catalysts with those of Cu(NPs) reported in the literature and this work.

Pollutant	Catalyst	k′ (s^{-1} g^{-1})	Time (min)	Conditions			Reference
				$NaBH_4$ (M)	Pollutant (M)	Catalyst Mass (mg)	
4-Nitrophenol (4-NP)	Cu10/MZ	5.00	10	0.0045	0.0000675	1	[22]
	Cu10/ZSM-5	1.17	50	0.0045	0.0000675	1	[22]
	CuO/TiO_2	6.46	8	0.014	0.00035	2	This work
	Cu NPs@Fe_3O_4-LS	1.87	3	0.125	0.00125	7	[4]
	MnO@Cu/C	17.33	1.5	0.0193	0.0008	4	[16]
	C@Cu	59.00	1	0.033	0.00014	1	[49]
	Cu-Ag/GP	0.40	10	0.0714	0.000857	10	[50]
	Cu-Ni/GP	0.60	7	0.0714	0.000857	10	[50]
	CuVOS@SiO_2-3	1.57	2	0.00528	0.00014377	5	[51]
	CuVOS-3	8.20	2	0.00582	0.000138	5	[52]
Methyl orange (MO)	C@Cu	62.00	1	0.033	0.000061	1	[49]
	CuO/TiO_2	8.98	7	0.014	0.00035	2	This work
	Cu-Ag/GP	0.77	4	0.0714	0.00004286	10	[50]
	Cu-Ni/GP	0.38	5	0.0714	0.00004286	10	[50]
	CuVOS@SiO_2-3	1.37	4	0.00528	0.0003055	5	[51]
	CuVOS-3	6.47	2	0.00582	0.00029	5	[52]

Table 3. Rate constants obtained for 4-NP reduction by wt.% CuO/TiO_2.

Catalyst	k_{app} (s^{-1})	k′ ($s^{-1}g^{-1}$)
5 wt.% CuO/TiO_2	0.00175	17.5
10 wt.% CuO/TiO_2	0.00175	8.7
20 wt.% CuO/TiO_2	0.00328	8.2
30 wt.% CuO/TiO_2	0.00308	5.1
40 wt.% CuO/TiO_2	0.00512	6.4

Table 4. Rate constants obtained for MO reduction by wt.% CuO/TiO_2.

Catalyst	k_{app} (s^{-1})	k′ ($s^{-1}g^{-1}$)
5 wt.% CuO/TiO_2	0.00150	15.0
10 wt.% CuO/TiO_2	0.00126	6.3
20 wt.% CuO/TiO_2	0.00479	12.0
30 wt.% CuO/TiO_2	0.00546	9.1
40 wt.% CuO/TiO_2	0.00727	8.9

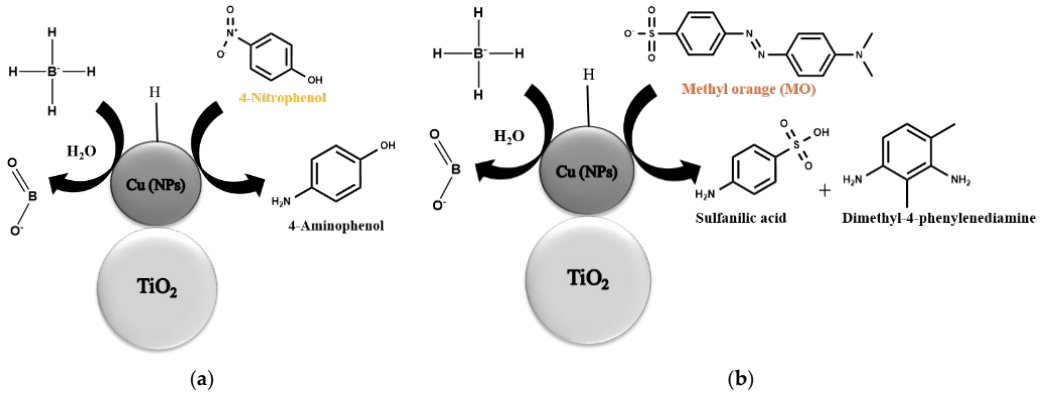

Figure 13. Schematic reactions of (**a**) 4-NP and (**b**) MO, by $NaBH_4$ in the presence of Cu(NPs)/TiO_2.

2.6.2. Effects of Parameters and Reusability

Multiple factors were investigated to understand their influence on the catalyzed reduction of 4-NP and MO using 40 wt.% CuO/TiO_2 catalysts. The parameters examined included the catalyst dosage and concentration of $NaBH_4$. Figure 14a,b show the impact of varying catalyst amounts on the rate of pollutant reduction. By making more active sites accessible for the reaction, the large amount of catalyst led to improved efficiency. The performance constantly increased as the catalyst amount increased from 0.02 g/L to 0.06 g/L, which confirms the principle of Sabatier [53]. The variation in $NaBH_4$ concentration had a pronounced influence on the catalytic reduction of 4-NP and MO (Figure 14c,d). Because of the limited quantity of hydrogen emitted, the catalytic reduction rate decreased as the $NaBH_4$ concentration decreased [54].

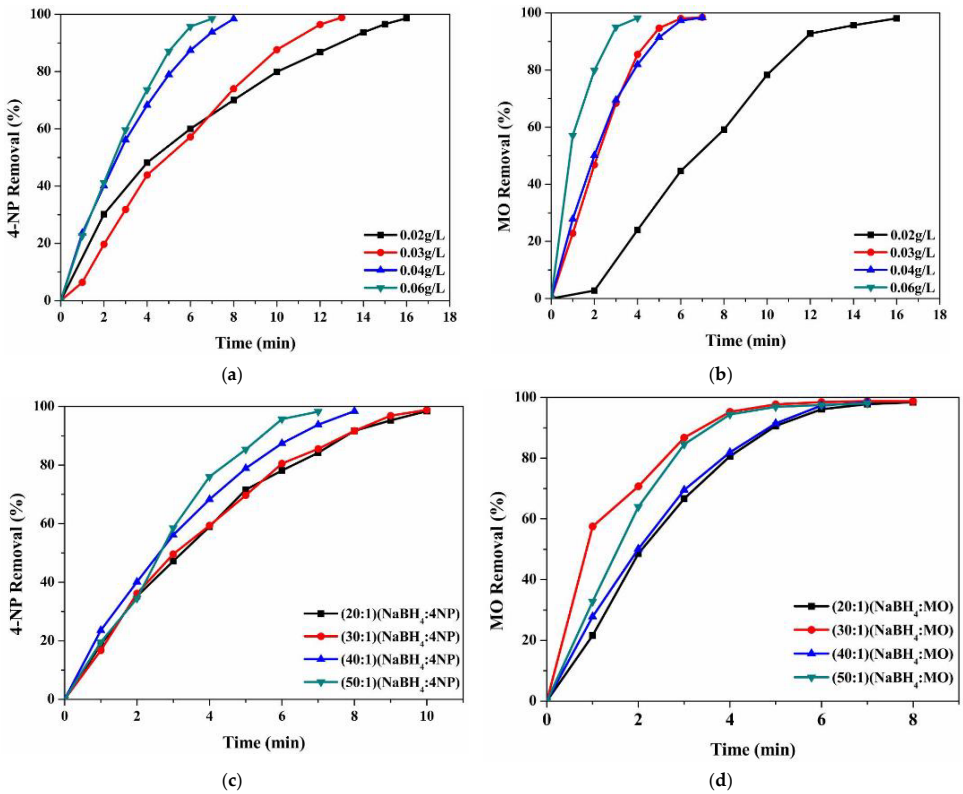

Figure 14. Pollutant removal versus time plots for catalytic reduction using 40 wt.% CuO/TiO_2, showing the effect of catalyst dose on the reduction of (**a**) 4-NP and (**b**) MO, and the effect of $NaBH_4$ concentration on the reduction of (**c**) 4-NP and (**d**) MO.

An essential characteristic of catalysts is their stability and reusability. To assess this, a fresh solution containing pollutants was introduced after each catalytic reduction cycle. The initial concentration remained constant at 0.35 mM throughout. As depicted in Figure 15a,b, the catalyst consistently maintained over 96% MO capacity and 94% 4-NP capacity for reduction of the dyes across 10 successive reaction cycles. This outcome highlights the exceptional reusability of the CuO/TiO_2 catalyst. This excellent reusability can be attributed to the even distribution and robust stability of Cu on the TiO_2 surface, which in turn provides a greater number of active sites for catalytic processes.

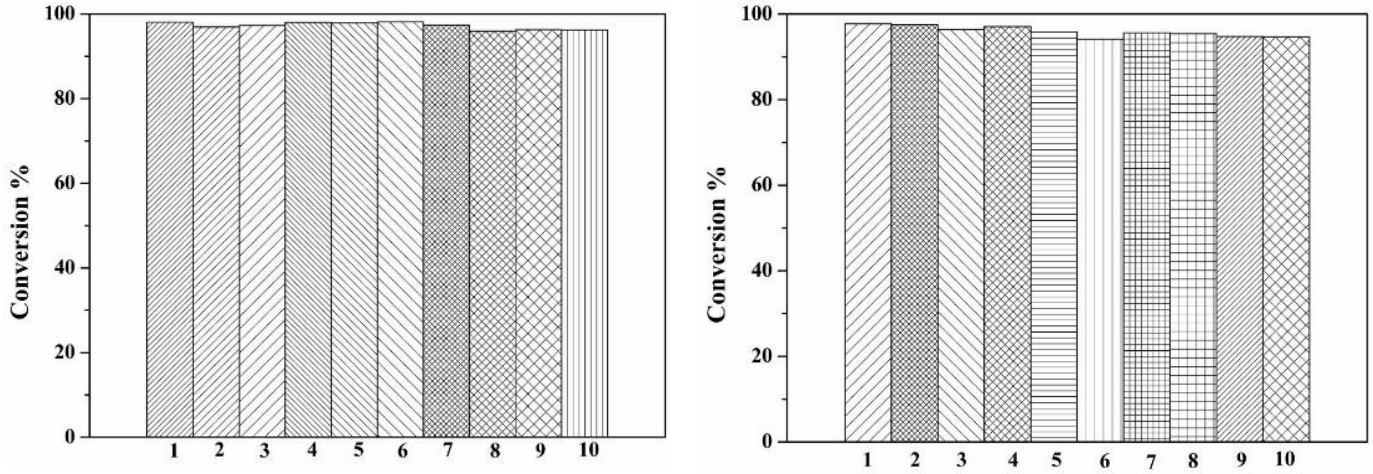

Figure 15. Recycling of CuO/TiO_2 in the hydrogenation of (**a**) 4-NP and (**b**) MO.

3. Materials and Methods

3.1. Synthesis of the CuO/TiO$_2$ Catalysts

The combustion technique was used to prepare different percentages of wt.% CuO/TiO_2 (wt = 5, 10, 20, 30, and 40%). Analytical grade $Cu(NO_3)_2{\cdot}6H_2O$ (Sigma Aldrich, ≥99.9%), along with TiO_2-P25 (Degussa Aeroxide P25) and citric acid as a fuel (Sigma Aldrich, ≥99.5%), served as the starting materials. Initially, these materials were added to deionized water with a fixed weight percentage of metal on TiO_2 and an excess amount of citric acid. The resulting mixtures were then stirred to achieve a well-dispersed suspension. The suspension subsequently underwent evaporation from 80 to 130 °C to yield a thick gel. This gel was subsequently converted into a dry form. Finally, the dry gel was calcined in an air atmosphere at 700 °C for 4 h with a ramp rate of 10 °C/min. Figure 16 represents the synthesis method for the catalysts.

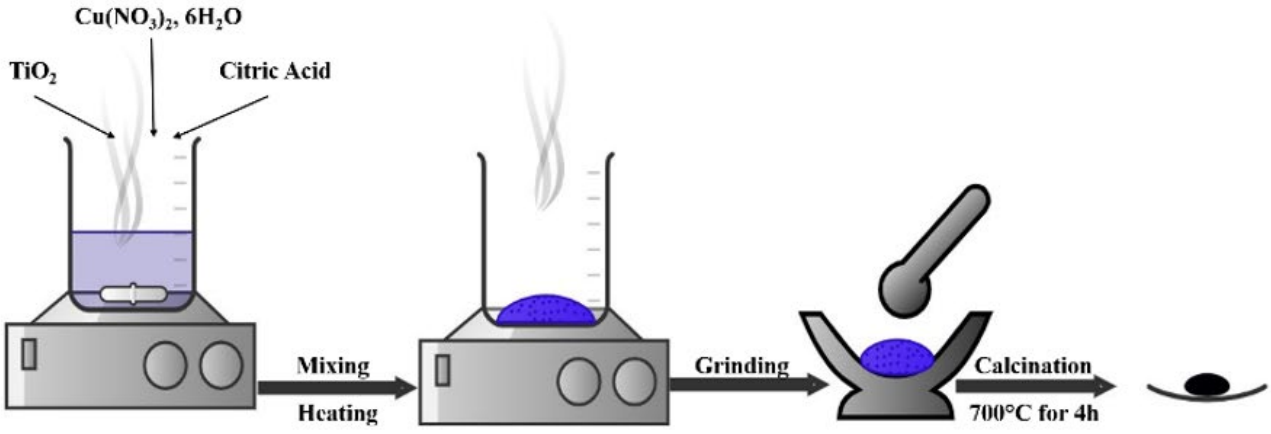

Figure 16. Synthesis procedure for the catalysts.

3.2. Catalytic Reduction of Organic Pollutants

The catalytic activity of CuO/TiO_2 was evaluated by studying the reduction of MO (Sigma Aldrich, ≥98.0%) and 4-nitrophenylphenol (Sigma Aldrich, ≥99.0%) as the target pollutants for the experiments. The experimental setup involved a beaker (50 mL) placed at room temperature. The catalytic reaction proceeded as follows: 2 mg of CuO/TiO_2 was uniformly dispersed in 35 mL of deionized water, followed by the addition of 10 mL of freshly prepared aqueous $NaBH_4$ (Sigma Aldrich, ≥99.0%) (70 mM). The solution was sonicated for 10 min, resulting in a color change from a black CuO/TiO_2 suspension to a gray color, indicating the formation of $Cu(NPs)/TiO_2$. Next, 5 mL of MO (3.5 mM) or 4-NP (3.5 mM) was added to the mixture. The overall concentrations of the organic dyes and $NaBH_4$ were 0.35 mM and 14 mM, respectively. The progress of the reaction was monitored by recording the time-dependent UV–vis absorption spectra of the reaction mixture in the wavelength range between 210 and 600 nm via a spectrophotometer (Techcomp UV 2300). The catalytic reduction experiment is shown in Figure 17.

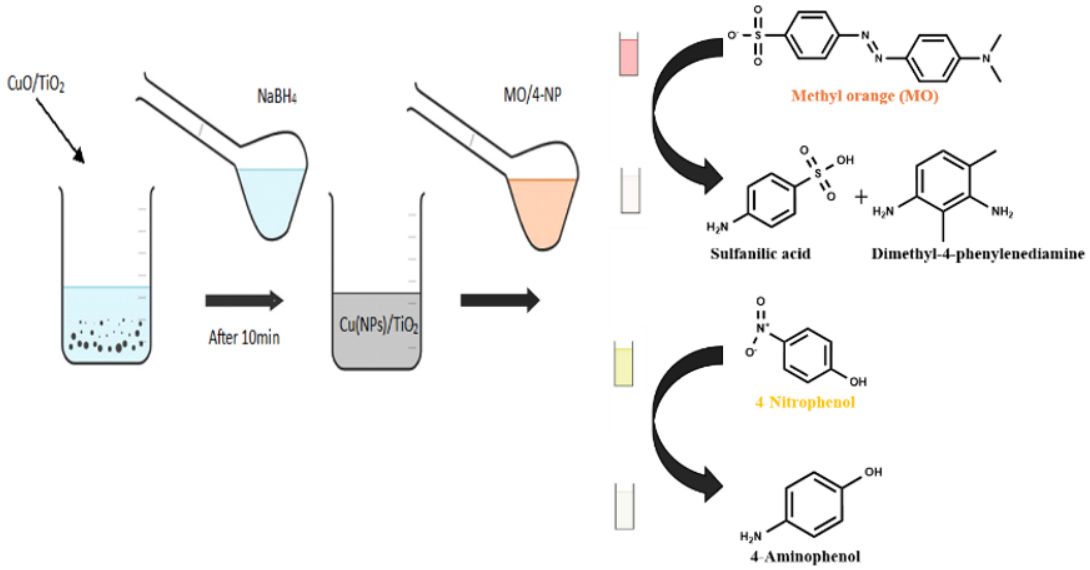

Figure 17. Catalytic reduction experiments of organic pollutants.

3.3. Characterization Techniques

The identification of the mineral crystalline phase of the catalysts was carried out via X-ray diffraction, via a Schimadzu 6100 powder diffractometer with a monochromatic beam ($\lambda_{Cuk\alpha}$ = 1.541838°). These measurements were taken at room temperature over a 2θ range of 10° to 70°, with a scanning rate of 2°/min. A UV–vis spectrophotometer, namely, a PerkinElmer Lamda 900 UV/Vis/NIR spectrometer, was used to obtain diffuse reflectance spectra of the catalysts in the wavelength range of 200–800 nm. To identify the main functional groups of the catalyst, ATR–FTIR spectroscopy was used with a Nicolet iS50 instrument with a resolution of 4 cm^{-1} in the spectral range of 400–4000 cm^{-1}. The thermal stability and degradation behavior of the catalysts were verified via simultaneous TGA and DTA under an air flow rate of 30 mL/min via a Labsys^{TM} (1F) Setaram instrument. An 8 mg sample was placed in an alumina crucible and heated from 30 °C to 800 °C at a heating rate of 10 °C/min. The surface morphology and chemical analysis of the samples were performed by SEM-EDX on a Quattros S-FEG-Thermofisher scientific instrument.

4. Conclusions

In this study, CuO/TiO_2 catalysts were prepared through a combustion technique. The catalysts were characterized via XRD, ATR–FTIR spectroscopy, TGA–DTA, UV–vis DRS, and SEM–EDX techniques. Compared with TiO_2 and CuO, the presence of Cu in the CuO/TiO_2 catalysts significantly enhanced the reduction of 4-NP and MO. The

fastest dye reduction was obtained with 40 wt.% CuO, followed by 40 > 30 > 20 > 10 > 5 wt.% CuO/TiO_2 in the presence of $NaBH_4$ and 2 mg of catalyst. The kinetic data were successfully modeled via the pseudo-first-order Langmuir–Hinshelwood mechanism, yielding rate constants of 0.000517 s^{-1} for 4-NP and 0.00727 s^{-1} for MO. The efficiency of 4-NP and MO reduction with the CuO/TiO_2 catalyst improved as the catalyst dosage increased from 0.02 g/L to 0.06 g/L, offering more active sites. However, a decrease in $NaBH_4$ concentration led to a decrease in the catalytic reduction rate due to reduced hydrogen production. The presence of TiO_2 rutile functions as a protective agent to slow catalyst damage and agglomeration of particles. This material can be reused for several cycles without significant loss of catalytic activity.

Author Contributions: Conceptualization, M.A.; methodology, M.A.; software, M.A. and B.H.; validation, A.B. and A.E.H.; formal analysis, M.A. and A.B.; investigation, M.A.; resources, A.E.H. and A.B.; data curation, M.A.; writing—original draft preparation, M.A.; writing—review and editing, A.B., F.Z., A.E.H., A.S., M.D., K.A., R.S. and L.R.; visualization F.Z., M.D. and L.R.; supervision, A.E.H., A.B., M.A.E.B. and M.M.A. All authors have read and agreed to the published version of the manuscript.

Funding: This research was supported by the Researchers Supporting Project number (RSPD2024R628), King Saud University, Riyadh, Saudi Arabia.

Institutional Review Board Statement: Not applicable.

Data Availability Statement: The data presented in this study are available upon request from the corresponding author.

Acknowledgments: The authors extend their appreciation to the Researchers Supporting Project number (RSPD2024R628), King Saud University, Riyadh, Saudi Arabia for supporting this research.

Conflicts of Interest: The authors declare no conflicts of interest.

References

1. Szymczyk, A.; van der Bruggen, B.; Ulbricht, M. Surface Modification of Water Purification Membranes. In *Surface Modification of Polymers*; John Wiley & Sons, Ltd.: Hoboken, NJ, USA, 2019; pp. 363–398. ISBN 978-3-527-81924-9.
2. Bilal, M.; Khan, S.; Ali, J.; Ismail, M.; Khan, M.I.; Asiri, A.M.; Khan, S.B. Biosynthesized Silver Supported Catalysts for Disinfection of Escherichia Coli and Organic Pollutant from Drinking Water. *J. Mol. Liq.* **2019**, *281*, 295–306. [CrossRef]
3. Ismail, M.; Khan, M.I.; Khan, S.B.; Akhtar, K.; Khan, M.A.; Asiri, A.M. Catalytic Reduction of Picric Acid, Nitrophenols and Organic Azo Dyes via Green Synthesized Plant Supported Ag Nanoparticles. *J. Mol. Liq.* **2018**, *268*, 87–101. [CrossRef]
4. Nezafat, Z.; Karimkhani, M.M.; Nasrollahzadeh, M.; Javanshir, S.; Jamshidi, A.; Orooji, Y.; Jang, H.W.; Shokouhimehr, M. Facile Synthesis of Cu NPs@Fe_3O_4-Lignosulfonate: Study of Catalytic and Antibacterial/Antioxidant Activities. *Food Chem. Toxicol.* **2022**, *168*, 113310. [CrossRef] [PubMed]
5. Munagapati, V.S.; Yarramuthi, V.; Kim, D.-S. Methyl Orange Removal from Aqueous Solution Using Goethite, Chitosan Beads and Goethite Impregnated with Chitosan Beads. *J. Mol. Liq.* **2017**, *240*, 329–339. [CrossRef]
6. Albukhari, S.M.; Ismail, M.; Akhtar, K.; Danish, E.Y. Catalytic Reduction of Nitrophenols and Dyes Using Silver Nanoparticles @ Cellulose Polymer Paper for the Resolution of Waste Water Treatment Challenges. *Colloids Surf. A Physicochem. Eng. Asp.* **2019**, *577*, 548–561. [CrossRef]
7. El-Aal, M.A.; Said, A.E.-A.A.; Goda, M.N.; Abo Zeid, E.F.; Ibrahim, S.M. Fe_3O_4@CMC-Cu Magnetic Nanocomposite as an Efficient Catalyst for Reduction of Toxic Pollutants in Water. *J. Mol. Liq.* **2023**, *385*, 122317. [CrossRef]
8. Ghorbani-Vaghei, R.; Veisi, H.; Aliani, M.H.; Mohammadi, P.; Karmakar, B. Alginate Modified Magnetic Nanoparticles to Immobilization of Gold Nanoparticles as an Efficient Magnetic Nanocatalyst for Reduction of 4-Nitrophenol in Water. *J. Mol. Liq.* **2021**, *327*, 114868. [CrossRef]
9. Kaid, M.; Ali, A.E.; Shamsan, A.Q.S.; Younes, S.M.; Abdel-Raheem, S.A.A.; Abdul-Malik, M.A.; Salem, W.M. Efficiency of Maturation Oxidation Ponds as a Post-Treatment Technique of Wastewater. *Curr. Chem. Lett.* **2022**, *11*, 415–422. [CrossRef]
10. Lajevardi, A.; Tavakkoli Yaraki, M.; Masjedi, A.; Nouri, A.; Hossaini Sadr, M. Green Synthesis of MOF@Ag Nanocomposites for Catalytic Reduction of Methylene Blue. *J. Mol. Liq.* **2019**, *276*, 371–378. [CrossRef]
11. Zhang, K.; Suh, J.M.; Choi, J.-W.; Jang, H.W.; Shokouhimehr, M.; Varma, R.S. Recent Advances in the Nanocatalyst-Assisted $NaBH_4$ Reduction of Nitroaromatics in Water. *ACS Omega* **2019**, *4*, 483–495. [CrossRef]
12. Landge, V.K.; Sonawane, S.H.; Manickam, S.; Bhaskar Babu, G.U.; Boczkaj, G. Ultrasound-Assisted Wet-Impregnation of Ag–Co Nanoparticles on Cellulose Nanofibers: Enhanced Catalytic Hydrogenation of 4-Nitrophenol. *J. Environ. Chem. Eng.* **2021**, *9*, 105719. [CrossRef]

13. Mekki, A.; Mokhtar, A.; Hachemaoui, M.; Beldjilali, M.; Meliani, M.F.; Zahmani, H.H.; Hacini, S.; Boukoussa, B. Fe and Ni Nanoparticles-Loaded Zeolites as Effective Catalysts for Catalytic Reduction of Organic Pollutants. *Microporous Mesoporous Mater.* **2021**, *310*, 110597. [CrossRef]
14. Omole, M.A.; K'Owino, I.O.; Sadik, O.A. Palladium Nanoparticles for Catalytic Reduction of Cr(VI) Using Formic Acid. *Appl. Catal. B Environ.* **2007**, *76*, 158–167. [CrossRef]
15. Saravanakumar, K.; Priya, V.S.; Balakumar, V.; Prabavathi, S.L.; Muthuraj, V. Noble Metal Nanoparticles (Mx = Ag, Au, Pd) Decorated Graphitic Carbon Nitride Nanosheets for Ultrafast Catalytic Reduction of Anthropogenic Pollutant, 4-Nitrophenol. *Environ. Res.* **2022**, *212*, 113185. [CrossRef]
16. Shokry, R.; Abd El Salam, H.M.; Aman, D.; Mikhail, S.; Zaki, T.; El Rouby, W.M.A.; Farghali, A.A.; Al Zoubi, W.; Ko, Y.G. MOF-Derived Core–Shell MnO@Cu/C as High-Efficiency Catalyst for Reduction of Nitroarenes. *Chem. Eng. J.* **2023**, *459*, 141554. [CrossRef]
17. Alencar, L.M.; Silva, A.W.B.N.; Trindade, M.A.G.; Salvatierra, R.V.; Martins, C.A.; Souza, V.H.R. One-Step Synthesis of Crumpled Graphene Fully Decorated by Copper-Based Nanoparticles: Application in H_2O_2 Sensing. *Sens. Actuators B Chem.* **2022**, *360*, 131649. [CrossRef]
18. Chaerun, S.K.; Prabowo, B.A.; Winarko, R. Bionanotechnology: The Formation of Copper Nanoparticles Assisted by Biological Agents and Their Applications as Antimicrobial and Antiviral Agents. *Environ. Nanotechnol. Monit. Manag.* **2022**, *18*, 100703. [CrossRef]
19. Cuong, H.N.; Pansambal, S.; Ghotekar, S.; Oza, R.; Thanh Hai, N.T.; Viet, N.M.; Nguyen, V.-H. New Frontiers in the Plant Extract Mediated Biosynthesis of Copper Oxide (CuO) Nanoparticles and Their Potential Applications: A Review. *Environ. Res.* **2022**, *203*, 111858. [CrossRef]
20. Godiya, C.B.; Kumar, S.; Park, B.J. Superior Catalytic Reduction of Methylene Blue and 4-Nitrophenol by Copper Nanoparticles-Templated Chitosan Nanocatalyst. *Carbohydr. Polym. Technol. Appl.* **2023**, *5*, 100267. [CrossRef]
21. Patil, D.; Manjanna, J.; Chikkamath, S.; Uppar, V.; Chougala, M. Facile Synthesis of Stable Cu and CuO Particles for 4-Nitrophenol Reduction, Methylene Blue Photodegradation and Antibacterial Activity. *J. Hazard. Mater. Adv.* **2021**, *4*, 100032. [CrossRef]
22. Aslam, S.; Subhan, F.; Waqas, M.; Zifeng, Y.; Yaseen, M.; Naeem, M. Cu Nanoparticles Confined within ZSM-5 Derived Mesoporous Silica (MZ) with Enhanced Stability for Catalytic Hydrogenation of 4-Nitrophenol and Degradation of Azo Dye. *Microporous Mesoporous Mater.* **2023**, *354*, 112547. [CrossRef]
23. Patra, A.K.; Dutta, A.; Bhaumik, A. Cu Nanorods and Nanospheres and Their Excellent Catalytic Activity in Chemoselective Reduction of Nitrobenzenes. *Catal. Commun.* **2010**, *11*, 651–655. [CrossRef]
24. Taherian, Z.; Khataee, A.; Han, N.; Orooji, Y. Hydrogen Production through Methane Reforming Processes Using Promoted-Ni/Mesoporous Silica: A Review. *J. Ind. Eng. Chem.* **2022**, *107*, 20–30. [CrossRef]
25. Wang, C.; Liu, Y.; Cui, Z.; Yu, X.; Zhang, X.; Orooji, Y.; Zhang, Q.; Chen, L.; Ma, L. In Situ Synthesis of Cu Nanoparticles on Carbon for Highly Selective Hydrogenation of Furfural to Furfuryl Alcohol by Using Pomelo Peel as the Carbon Source. *ACS Sustain. Chem. Eng.* **2020**, *8*, 12944–12955. [CrossRef]
26. Ningsih, L.A.; Yoshida, M.; Sakai, A.; Andrew Lin, K.-Y.; Wu, K.C.W.; Catherine, H.N.; Ahamad, T.; Hu, C. Ag-Modified $TiO_2/SiO_2/Fe_3O_4$ Sphere with Core-Shell Structure for Photo-Assisted Reduction of 4-Nitrophenol. *Environ. Res.* **2022**, *214*, 113690. [CrossRef]
27. Tran, X.T.; Hussain, M.; Kim, H.T. Facile and Fast Synthesis of a Reduced Graphene Oxide/Carbon Nanotube/Iron/Silver Hybrid and Its Enhanced Performance in Catalytic Reduction of 4–Nitrophenol. *Solid State Sci.* **2020**, *100*, 106107. [CrossRef]
28. Zhao, X.; Lv, L.; Pan, B.; Zhang, W.; Zhang, S.; Zhang, Q. Polymer-Supported Nanocomposites for Environmental Application: A Review. *Chem. Eng. J.* **2011**, *170*, 381–394. [CrossRef]
29. Bakhsh, E.M.; Khan, S.B.; Maslamani, N.; Danish, E.Y.; Akhtar, K.; Asiri, A.M. Carboxymethyl Cellulose/Copper Oxide–Titanium Oxide Based Nanocatalyst Beads for the Reduction of Organic and Inorganic Pollutants. *Polymers* **2023**, *15*, 1502. [CrossRef]
30. Liao, X.; Zheng, L.; He, Q.; Li, G.; Zheng, L.; Li, H.; Tian, T. Fabrication of Ag/TiO_2 Membrane on Ti Substrate with Integral Structure for Catalytic Reduction of 4-Nitrophenol. *Process Saf. Environ. Prot.* **2022**, *168*, 792–799. [CrossRef]
31. Hassan, F.; Abbas, A.; Ali, F.; Nazir, A.; Al Huwayz, M.; Alwadai, N.; Iqbal, M.; Ali, Z. Bio-Mediated Synthesis of Cu-TiO_2 Nanoparticles Using *Phoenix Dactylifera* Lignocellulose as Capping and Reducing Agent for the Catalytic Degradation of Toxic Dyes. *Desalination Water Treat.* **2023**, *298*, 53–60. [CrossRef]
32. Kaur, R.; Pal, B. Cu Nanostructures of Various Shapes and Sizes as Superior Catalysts for Nitro-Aromatic Reduction and Co-Catalyst for Cu/TiO_2 Photocatalysis. *Appl. Catal. A Gen.* **2015**, *491*, 28–36. [CrossRef]
33. Akbari, R. Green Synthesis and Catalytic Activity of Copper Nanoparticles Supported on TiO_2 as a Highly Active and Recyclable Catalyst for the Reduction of Nitro-Compounds and Degradation of Organic Dyes. *J. Mater. Sci. Mater. Electron.* **2021**, *32*, 15801–15813. [CrossRef]
34. Khodadadi, B.; Yeganeh Faal, A.; Shahvarughi, A. Tilia Platyphyllos Extract Assisted Green Synthesis of CuO/TiO2 Nanocomposite: Application as a Reusable Catalyst for the Reduction of Organic Dyes in Water. *Journal of Applied Chemical Research* **2019**, *13*, 51–65.
35. Tian, X.; Dong, Y.; Zahid, M. One-Pot Synthesis of CuO/TiO Nanocomposites for Improved Photocatalytic Hydrogenation of 4-Nitrophenol to 4-Aminophenol under Direct Sunlight. *J. Chin. Chem. Soc.* **2023**, *70*, 848–856. [CrossRef]

36. Li, P.; Zhang, X.; Wang, J.; Xu, B.; Zhang, X.; Fan, G.; Zhou, L.; Liu, X.; Zhang, K.; Jiang, W. Binary CuO/TiO_2 Nanocomposites as High-Performance Catalysts for Tandem Hydrogenation of Nitroaromatics. *Colloids Surf. A Physicochem. Eng. Asp.* **2021**, *629*, 127383. [CrossRef]
37. Monshi, A.; Foroughi, M.R.; Monshi, M. Modified Scherrer Equation to Estimate More Accurately Nano-Crystallite Size Using XRD. *World J. Nano Sci. Eng.* **2012**, *2*, 154–160. [CrossRef]
38. Hanaor, D.A.H.; Sorrell, C.C. Review of the Anatase to Rutile Phase Transformation. *J. Mater. Sci.* **2011**, *46*, 855–874. [CrossRef]
39. Ha, C.A.; Nguyen, D.T.; Nguyen, T. Green Fabrication of Heterostructured $CoTiO_3$/TiO_2 Nanocatalysts for Efficient Photocatalytic Degradation of Cinnamic Acid. *ACS Omega* **2022**, *7*, 40163–40175. [CrossRef]
40. Lin, Y.-J.; Chang, Y.-H.; Yang, W.-D.; Tsai, B.-S. Synthesis and Characterization of Ilmenite $NiTiO_3$ and $CoTiO_3$ Prepared by a Modified Pechini Method. *J. Non-Cryst. Solids* **2006**, *352*, 789–794. [CrossRef]
41. Bopape, D.A.; Mathobela, S.; Matinise, N.; Motaung, D.E.; Hintsho-Mbita, N.C. Green Synthesis of CuO-TiO_2 Nanoparticles for the Degradation of Organic Pollutants: Physical, Optical and Electrochemical Properties. *Catalysts* **2023**, *13*, 163. [CrossRef]
42. Shi, Q.; Li, Y.; Zhan, E.; Ta, N.; Shen, W. Anatase TiO_2 Hollow Nanosheets: Dual Roles of F−, Formation Mechanism, and Thermal Stability. *CrystEngComm* **2014**, *16*, 3431–3437. [CrossRef]
43. Li, B.; Hao, Y.; Zhang, B.; Shao, X.; Hu, L. A Multifunctional Noble-Metal-Free Catalyst of CuO/TiO_2 Hybrid Nanofibers. *Appl. Catal. A Gen.* **2017**, *531*, 1–12. [CrossRef]
44. Angel, R.D.; Durán-Álvarez, J.C.; Zanella, R.; Angel, R.D.; Durán-Álvarez, J.C.; Zanella, R. TiO2-Low Band Gap Semiconductor Heterostructures for Water Treatment Using Sunlight-Driven Photocatalysis. In *Titanium Dioxide—Material for a Sustainable Environment*; IntechOpen: London, UK, 2018; ISBN 978-1-78923-327-8.
45. Sirohi, S.; Mittal, A.; Nain, R.; Jain, N.; Singh, R.; Dobhal, S.; Pani, B.; Parida, D. Effect of Nanoparticles Shape on Conductivity of Ag Nanoparticle PVA Composite Films. *Polym. Int.* **2019**, *68*, 1961–1967. [CrossRef]
46. Vidhu, V.K.; Philip, D. Catalytic Degradation of Organic Dyes Using Biosynthesized Silver Nanoparticles. *Micron* **2014**, *56*, 54–62. [CrossRef] [PubMed]
47. Li, X.; Ma, Y.; Yang, Z.; Huang, D.; Xu, S.; Wang, T.; Su, Y.; Hu, N.; Zhang, Y. In Situ Preparation of Magnetic Ni-Au/Graphene Nanocomposites with Electron-Enhanced Catalytic Performance. *J. Alloys Compd.* **2017**, *706*, 377–386. [CrossRef]
48. Lin, F.; Doong, R. Bifunctional Au−Fe3O4 Heterostructures for Magnetically Recyclable Catalysis of Nitrophenol Reduction. *J. Phys. Chem. C* **2011**, *115*, 6591–6598. [CrossRef]
49. Ahsan, M.A.; Jabbari, V.; El-Gendy, A.A.; Curry, M.L.; Noveron, J.C. Ultrafast Catalytic Reduction of Environmental Pollutants in Water via MOF-Derived Magnetic Ni and Cu Nanoparticles Encapsulated in Porous Carbon. *Appl. Surf. Sci.* **2019**, *497*, 143608. [CrossRef]
50. Ismail, M.; Khan, M.I.; Khan, S.B.; Khan, M.A.; Akhtar, K.; Asiri, A.M. Green Synthesis of Plant Supported CuAg and CuNi Bimetallic Nanoparticles in the Reduction of Nitrophenols and Organic Dyes for Water Treatment. *J. Mol. Liq.* **2018**, *260*, 78–91. [CrossRef]
51. Sun, H.; Abdeta, A.B.; Zelekew, O.A.; Guo, Y.; Zhang, J.; Kuo, D.-H.; Lin, J.; Chen, X. Spherical Porous SiO_2 Supported CuVOS Catalyst with an Efficient Catalytic Reduction of Pollutants under Dark Condition. *J. Mol. Liq.* **2020**, *313*, 113567. [CrossRef]
52. Sun, H.; Zelekew, O.A.; Chen, X.; Guo, Y.; Kuo, D.-H.; Lu, Q.; Lin, J. A Noble Bimetal Oxysulfide CuVOS Catalyst for Highly Efficient Catalytic Reduction of 4-Nitrophenol and Organic Dyes. *RSC Adv.* **2019**, *9*, 31828–31839. [CrossRef]
53. Ahmad, S.; Khan, S.B.; Asiri, A.M. Catalytic Efficiency of Copper Nanoparticles Modified Silica-Alginate Hydrogel Nanocomposite towards Reduction of Water Pollutants and H_2 Generation. *Int. J. Hydrogen Energy* **2023**, *48*, 6399–6417. [CrossRef]
54. Yang, K.; Yan, Y.; Wang, H.; Sun, Z.; Chen, W.; Kang, H.; Han, Y.; Zahng, W.; Sun, X.; Li, Z. Monodisperse Cu/Cu_2O@C Core–Shell Nanocomposite Supported on RGO Layers as an Efficient Catalyst Derived from a Cu-Based MOF/GO Structure. *Nanoscale* **2018**, *10*, 17647–17655. [CrossRef] [PubMed]

Disclaimer/Publisher's Note: The statements, opinions and data contained in all publications are solely those of the individual author(s) and contributor(s) and not of MDPI and/or the editor(s). MDPI and/or the editor(s) disclaim responsibility for any injury to people or property resulting from any ideas, methods, instructions or products referred to in the content.